ACTA CHEMICA SCANDINAVICA 22 (1968) 1509–1531

A Non-Equilibrium Low Vapor Pressure Heat of Vaporization Calorimeter

Part I. Vapor Pressure Range 200—10^{-3} mm Hg

ERNST MORAWETZ

Thermochemistry Laboratory, University of Lund, Lund, Sweden*

A micro heat of vaporization calorimeter was constructed and tested at 25°C under various vapor flow conditions in the vapor pressure range 200—10^{-3} mm Hg. Twelve liquid and solid test substances with known enthalpies of vaporization were used.

The errors in the experimental values varied between *ca.* 0 and 590 cal/mole. Deviations of this magnitude were expected since the evaporation inside the calorimeter took place against pressures smaller than or equal to saturation pressure. Consequently, the pressure-volume work performed was less than $P\Delta V = RT_0 = 590$ cal/mole. A simple expression was derived for the calculation of the deviations in terms of the local flow Mach number, Ma, which allowed the prediction of three regions of error, $\delta\Delta H_v$:

a) $\delta\Delta H_v \rightarrow 0$ for Ma$\rightarrow$0, *i.e.* $P\Delta V \rightarrow RT_0$,
b) $\delta\Delta H_v \rightarrow$ *ca.* 230 cal/mole (25°C) for Ma$=$1, *i.e.* the maximum attainable Mach number in the continuum flow of evaporating molecules,
c) $\delta\Delta H_v \rightarrow RT_0 = 590$ cal/mole (25°C) for Ma$\rightarrow\infty$ in non-continuum flow (molecular flow), *i.e.* $P\Delta V \rightarrow 0$.

All three limiting values could be experimentally verified within the limits of error.

The method developed allows the determination of unknown vaporization enthalpies by operating at an accessible limiting flow Mach number, in the pressure range 200—10^{-2} mm Hg and in the pressure range 10^{-2}—10^{-3} mm Hg with an accuracy of *ca.* $\pm$40 cal/mole and $\pm$80 cal/mole, respectively.

* Sponsored by the *Swedish Natural Science Research Council* and the *Swedish Council for Applied Research.*

The construction and testing of an isothermal micro-calorimeter has been described earlier.[1] It has been used for the determination of heats of vaporization of organic substances exerting vapor pressures in the range of 1 to 10^{-2} mm Hg at 25°C. The precision of the measured heats of vaporization was satisfactory over the total pressure range. The data obtained were associated with a systematic error which limited the usefulness of the method, especially in the low pressure range. By applying a minor empirical correction it was possible to obtain data accurate to within 0.1 kcal/mole. It was, however, uncertain whether this correction also applied for solid substances.

The method looked promising and it was felt that further systematic studies may lead to improvements. It was also desirable to extend the pressure range to pressures lower than 10^{-2} mm Hg. Also, it appeared possible to reduce the systematic error by firstly gaining a deeper insight into its physical nature by a more thorough study of the vapor flow behavior, and secondly by improving the system design and diminishing heat leakages.

In order to get more information on the final thermodynamic state of evaporation it was of particular interest to investigate the way in which the nature of the vapor flow influences the equilibrium pressure in the calorimeter chamber and, hence, the heat of vaporization.

GENERAL CONSIDERATIONS

The influence of the external pressure upon the vaporization process. The enthalpy change on vaporization at equilibrium conditions derives from the definition of enthalpy $H=E+PV$,

$$\Delta H_v = \Delta E_v + P_0(V_g - V_l)T_0 \tag{1}$$

where ΔE_v is the internal energy change at temperature T_0, and $P_0(V_g-V_l)T_0$ is the pressure-volume work performed by the evaporating molecules against the saturation pressure $P_0=P_{sat}$ on passing from the liquid to the gaseous phase. The volume difference $(V_g-V_l)T_0$ accounts for the volume change associated with the evaporation process.

For external pressures $P_{ex}=P_1<P_{sat}=P_0$ the enthalpy change is more generally given by

$$\Delta H_v' = \Delta E_v'(P_{ex}) + P_{ex}(V_g - V_l)T_0 < \Delta H_v \tag{2}$$

where the dependence of the measurable $\Delta H_v'$-value on the prevailing external pressure is explicitly expressed. The change in the internal energy is now given by

$$\Delta E_v' = \Delta E_v + \int_{P_{sat}=P_0}^{P_{ex}=P_1} \left(\frac{dE}{dP}\right)_{T_0} dP$$

$$= \Delta E_v + \int_{P_0}^{P_1} \left(\frac{dE}{dV}\right)_{T_0} \left(\frac{dV}{dP}\right)_{T_0} dP \tag{3}$$

Substituting eqn. (3) into eqn. (2),

$$\Delta H_v' = \Delta E_v + \int_{P_0}^{P_1} \left(\frac{dE}{dV}\right)_{T_0} \left(\frac{dV}{dP}\right)_{T_0} dP + P_1(V_g - V_l)T_0 \quad (4)$$

At the low absolute pressures considered in this work, the vapor can be treated as an ideal gas. Hence, the integral is zero and $\Delta E_v' = \Delta E_v$. Neglecting V_l, as compared with V_g, the PV-work at equilibrium is

$$P_0(V_g - V_l)T_0 \approx RT_0 \quad (5)$$

Substituting the volume difference from this equation into eqn. (4) gives

$$\Delta H_v' = \Delta E_v + RT_0 \cdot P_1/P_0 \quad (6)$$

In the limit, when the external pressure $P_{ex}=P_1$ approaches zero, the PV-work vanishes.[2] When $P_{ex}=P_{sat}=P_0$,

$$\Delta H_v' = \Delta E_v + RT_0 = \Delta H_v \quad (7)$$

Substituting ΔE_v from eqn. (6) into eqn. (7) and rearranging, a simple equation is obtained, which expresses an observable enthalpy difference, $\delta\Delta H_v$, in terms of the external pressure $P_{ex}=P_1$ on the liquid surface,

$$\delta\Delta H_v = \Delta H_v - \Delta H_v' = (1 - P_1/P_0)RT_0 \quad (8)$$

This equation is generally valid assuming that ideal gas conditions prevail. $\Delta H_v'$ corresponds to the experimental datum and ΔH_v to the equilibrium datum, which for a test substance may be taken equal to the "literature" value. Hence, the difference, $\delta\Delta H_v$, appears as a systematic error associated with the experimental determination of the vaporization enthalpy.

Factors governing the mass flow on vaporization. As the existence of a mass flow is a prerequisite for the heat of vaporization experiment to be performed, and simultaneously may be the cause for a discrepancy in the observed enthalpy of vaporization value, it is necessary to discuss in greater detail the effects of the mass flow on the measured vaporization enthalpies.

The steady state mass flow of vapor from an open isothermal enclosure containing an evaporating surface, a vapor phase and a flow channel is governed by two factors:

a) the emissive properties of the surface, which depend upon parameters such as the absolute emissivity, the condensation coefficient, the Knudsen number * (or the Reynolds number **) and the Mach number *** of the mass flow in the enclosure,

---

* The Knudsen number Kn is defined as the ratio of the mean free path λ to a characteristic dimension, *e.g.* the diameter d of a flow channel, $Kn \equiv \lambda/d$.

** The Reynolds number Re is defined by $Re \equiv \varrho v l/\eta$, where ϱ is the fluid density, v the fluid flow velocity, l the length of the flow channel and η the fluid viscosity.

*** The Mach number Ma is defined as the ratio of the fluid flow velocity v to the local speed of sound a, $Ma \equiv v/a$. The three flow parameters are interlinked by the expression [3,4] $Kn = f(K)Ma/Re$, where $f(K)$ is a function of $K = C_p/C_v$, its numerical value being of the order of unity.

b) the transmissive properties of the flow channel, which depend upon the geometry of the flow channel, the pressure ratio P/P_0 of downstream to upstream pressure, the Knudsen number (or the Reynolds number) and the Mach number of the mass flow through the channel.

The most important parameter for the present work, the ratio P_1/P_0, can be expected to be in some way dependent on the flow parameters common for both inflow and outflow, *i.e.* the Mach number Ma (or the Reynolds number Re) and the Knudsen number Kn.

Compressibility effects. One of the most important features of gas flow is the dependence of the gas density on the gas flow velocity, from which the compressibility of gases results.

In compressible fluid flow the pressure P is a function of the gas density and hence of the flow velocity. For a one-dimensional steady flow of an invisced compressible fluid the pressure P, can be expressed in terms of the pressure P_0 at flow speed zero and of the local flow Mach number Ma [5-7]

$$P_1 = P_0[1 + \mathrm{Ma}_1^2\,(K-1)/2]^{-K(K-1)} \tag{9}$$

For large molecules K approaches unity. In this case it can be shown that eqn. (9) may be replaced by

$$P_1 = P_0\,\exp(-\tfrac{1}{2}\,\mathrm{Ma}_1^2) \tag{10}$$

when the expression in paranthesis is expanded binomially. In fact, this equation only applies to isothermal compressible fluid flow, which represents a situation that is unattainable in this context. Nevertheless, it provides information about the general behaviour of eqn. (9).

The emissive properties of an evaporating surface. From elementary kinetic theory it is known that the maximum rate of emission of molecules by vaporization is given by the expression

$$\dot{m} = \alpha \cdot A \cdot v_a \cdot P_0/4RT_0 \text{ [mole/sec]} \tag{11}$$

when α, the evaporation or condensation coefficient (which is commonly assumed to be equal) is equal to unity. Here A is the evaporation surface area, and $v_a=(8\ RT_0/\pi\ M)^{\frac{1}{2}}$ is the average molecular velocity at temperature T_0.

It is usually assumed that for most simple liquids the value of α is close to unity,[8] whereas for solids there is some evidence of a pressure dependence.[9] At equilibrium the condensation coefficient may be very small, approaching unity only when the static pressure in the vapor phase is reduced.

The influence of the mass flow velocity on the emissive properties of an evaporating surface has been discussed by Crout [10] and Schrage.[11] By applying the kinetic theory to the problems of evaporation of mono- and polyatomic molecules, Crout showed that as evaporation occurs the distribution of molecular velocities close to the evaporating surface could not be Maxwellian. He suggested that the state of the non-isotropic vapor at the interface may be expressed by a "longitudinal temperature" in the direction of the evaporation, and a "transverse temperature" parallel to the surface.

A normal equipartition of energy in the vapor phase will first be established after a few mean free paths. This statement is, however, only justified, if, firstly the vapor space has a minimum dimension of at least three mean free paths [12] and, secondly, if relaxation effects can be neglected in the internal energy distribution among translational, rotational, and vibrational degrees of freedom. Relaxation effects may be caused by the rapid change of state associated with evaporation. In the present case these effects may be neglected,[3] if the Knudsen number of the evaporation chamber $Kn < 0.3$.

A further important consequence of Crout's theory is that the rate of evaporation from a flat surface is limited by the velocity of sound in the vapor. This implies, that when the pressure of the vapor phase into which the molecules evaporate is lowered, the mass flow velocity and hence the flow Mach number increases until a critical value is reached when the flow velocity of the isotropic vapor has become sonic and $Ma=1$. A further reduction in the pressure neither increases the rate of evaporation nor the mass flow velocity.

Crout showed that the rate of evaporation at the critical state is exceeded when the evaporated molecules are condensed at a distance smaller than the distance required to establish a Maxwellian velocity distribution. It is clear, that in the limit, when no intermolecular collisions occur and no molecules return to the surface, the maximum rate of evaporation, as given by eqn. (11), should be reached. In this situation, however, the velocity of sound in the vapor flow is zero, which corresponds to a flow Mach number $Ma \rightarrow \infty$. The static external pressure on the liquid surface is also zero, and from eqn. (8) the value of $\delta \Delta \bar{H}_v$ equals RT_0.

Conversely, if the time spent in the vapor phase exceeds the relaxation time, the flow Mach number cannot exceed unity. Hence, when this situation is reached, the value of the static pressure and of $\delta \Delta H_v$ reaches a limiting value.

Furthermore, if the flow Mach number of the isotropic vapor equals zero, the vaporization occurs at the saturation pressure and $\delta \Delta H_v$ also equals zero.

This dependence of $\delta \Delta H_v$ on the Mach number can be expressed mathematically by substituting eqn. (9) or (10) into eqn. (8) yielding for the reduced ΔH_v-difference

$$\delta \Delta H_{red.} = \delta \Delta H_v / RT_0 = 1 - [1 + Ma_1^2(K-1)/2]^{-K/(K-1)} \qquad (12)$$

or, for $K \rightarrow 1$

$$\delta \Delta H_{red.} = 1 - \exp(-\tfrac{1}{2} Ma_1^2) \qquad (13)$$

It is apparent that $\Delta H_{red.}$ approaches zero, when Ma_1 tends to zero. When $Ma_1 = 1$, the limiting value for isotropic vaporization is $\Delta H_{red.} = 0.395$. When $Ma_1 \rightarrow \infty$, $\Delta H_{red.}$ approaches unity.*

* For reasons of comparison the functions (12) and (13) were plotted in the transonic range for $K=1.0$, $K=1.05$ (organic compounds), and $K=1.2$ (water). It became obvious that the difference between the limiting values at $Ma=1$ for the actual K-values and $K=1$ were negligible, especially for $K=1.05$. It is therefore justified to use eqn. (13) for approximate calculations instead of the more complex eqn. (12).

The transmissive properties of flow channels. Mass flow through a nozzle. In this work circular tubes and orifices of various length-to-diameter ratios (l/d) were employed as flow channels (Table 1). These channel types differ in their geometry in some very important aspects from a smooth convergent nozzle. However, a prior discussion of the flow behaviour in a convergent nozzle is useful, since the theoretical treatment of ideal nozzle flow is simple and reveals essential features, which are valid, at least approximately, for fluid flow through pipes and orifices.

When the theory of compressible flow is applied to one-dimensional flow through a convergent nozzle, it is found that for a certain "critical" pressure ratio of downstream to upstream pressure, P^*/P_0, the flow Mach number becomes unity at the nozzle throat and the mass flow reaches a maximum. This implies that the flow speed has reached the local velocity of sound at the throat. In this state the influence of the downstream pressure ceases altogether, and a further reduction in the pressure ratio can neither increase the critical Mach number, nor the critical mass flow. Hence the latter achieves a constant value.†

Another important aspect of the theory is the criterion that the flow speed becomes sonic at the throat (for $P_1/P_0 \leqslant P^*/P_0$), irrespective of whether the velocity of the flow, approaching the nozzle, is subsonic or supersonic. If the flow velocity upstream of the nozzle is sonic, it will not be changed.

Mass flow through orifices and circular pipes. So far the steady flow has been assumed to be isentropic and one-dimensional. This is an idealization which under certain circumstances can be approached in nozzle flow. If, however, the flow passes through a sharp-edged orifice or a re-entrant orifice (Borda tube), lacking the smooth inlet geometry of a nozzle, and if viscosity and friction effects are taken into consideration, the flow becomes adiabatic and two- or three-dimensional. Similar aspects are also valid for flow through short cylindrical pipes.

Liepmann[3] pointed out that the flow near the sharp edge of an orifice is locally two-dimensional, and, when the critical pressure ratio (eqn. 14) is reached, partially subsonic and partially supersonic. Since the mass flow becomes a maximum at local sonic velocity, the mass flow through an orifice must be less than through a comparable smooth nozzle. This fact is usually accounted for by multiplying the theoretical equations for the critical mass flow by a discharge coefficient $c<1$. It is known that the discharge coefficient increases as the pressure ratio is reduced.[14] This increase continues even after the critical pressure is reached as part of the flow is still subsonic. Experimentally it was found that maximum flow was first reached at considerably smaller pressure ratios than predicted by theory. Thus, for nitrogen flow through orifices[3] with $l/d=0.025$ and short tubes[15] with $0.005>l/d<1$, pressure ratios of less than 0.04 were required to approach maximum flow, as compared with the theoretical value 0.53 ($K=1.4$) for ideal nozzle flow. Such a small critical pressure ratio corresponds, according to eqn. (9), to a critical Mach number $\mathrm{Ma}^*=2.76$ ($K=1.40$), instead of $\mathrm{Ma}^*=1$.

† Expressions for the calculation of the critical pressure ratio and the critical mass flow are given in all standard works of gas dynamics.[5-7]

The same conclusion concerning the critical pressure ratio was reached by Oswatitsch,[6] who discussed the experimental results of Frössel [16] on subsonic and supersonic flow of air through cylindrical pipes with $0.32 > l/d < 360$ at high Reynold numbers. It was observed, that for subsonic flow sonic speed could be reached at the end of the pipe, only if the pressure ratio was sufficiently low.

The concept of a high velocity region. Jobson [17] suggested a method by which the variation of the discharge coefficient for incompressible flow at low Reynold numbers as a function of the pressure ratio could be calculated. The method was successfully improved by Bragg [18] to flows, in which upstream of the orifice compressibility effects could not be neglected.

His theory concerning the variation of the flow pattern upstream of the orifice has for this work, several interesting and important features. He states that under steady flow conditions the pressure acting over most of the walls of the reservoir is the stagnation pressure P_0. In the vicinity of the orifice, however, the fluid is in motion towards the outlet and the wall pressure is locally reduced. As long as the flow velocity is comparatively small, the flow upstream of the orifice behaves like an incompressible fluid, and the local wall velocities will be proportional to the mass flow. For this situation the coefficient is small, its limiting minimum value [19] being $\pi/(2+\pi)$. If, however, the discharge coefficient is considerably higher ($c > 0.7$), the flow upstream of the orifice will be affected by compressibility. Under such circumstances an increase in total flow does not increase all the local velocities in the same proportion. The increase in velocity and corresponding decrease in pressure will be proportionally greatest at points where the velocity is closest to the sonic value. This will, however, be the case along the orifice centerline, as theoretical calculations for orifice flow have shown.[20]

From this exposition the important conclusion is reached that upstream of the orifice exists a spatial region in which considerable changes in flow velocity occur. At low flow Mach numbers, this region (termed *high velocity region*) may be conceived as longitudinally restricted. When the Mach number increases, however, the high velocity region grows in size, most noticeably along the orifice center line. It can be expected that in subsonic flow through channels with increasing ratio l/r (pipes) the extent of the high velocity region diminishes, since maximum speed (sonic speed) can only be attained at the channel outlet.

It is convenient to view this region as being enveloped by a velocity hyper surface uniting all points upstream of the orifice having a common specific velocity. This velocity hyper surface may be characterized by a flow Mach number which is conveniently chosen as $Ma = 1/3$. This value is considered as a practical upper limit for incompressible flow. If $Ma > 1/3$, compressibility effects can no longer be neglected.[21]

A simple model for vaporization through flow channels into a vacuum. It is now possible to construct a simple theoretical model from which the variation of the enthalpy of vaporization on expanding the vapor through a flow channel into a near-vacuum space, may be demonstrated. The underlying theory is based on the following assumptions:

a) the vapor may be treated as an ideal gas,
b) Crout's theory applies,
c) a high velocity region, as defined above, exists upstream from the flow channel,
d) the vertical extent of this region becomes a maximum for $Ma_2 \rightarrow 1$ and $l/r \rightarrow 0$, and approaches zero for $Ma_2 \rightarrow 0$ and $l/r \rightarrow \infty$,†
e) eqns. 8, 12, and 13, respectively, apply.

An open system model as depicted in Fig. 1 can be used to study the influence of the model geometry, in terms of various Knudsen numbers, on the enthalpy of vaporization. In order to reveal the essential features it is assumed, that some time after opening the flow channel a steady flow state is reached. Hence, vapor will be discharged from the vaporization chamber through the channel at a constant rate and will enter the pumping line at local sonic speed, since the pressure is kept at a value $P<P^*$. The initial state of the vapor, before opening the channel, is always characterized by the stagnation parameters (suffix zero): Pressure P_0, temperature T_0, mean free path λ_0, Knudsen number for the chamber Kn_0, Mach number $Ma_0 = 0$.

The corresponding flow parameters are indicated by the suffix 1 for the flow in the evaporation chamber, and by the suffix 2 for the flow in the channel. The channel diameter d is always assumed to be much smaller than the chamber diameter, $d \ll D$.

On moving the piston (vaporization chamber bottom with sample) upwards, whilst vapor is being issued, it is possible to discern three distinct flow patterns associated with an equal number of limiting flow Mach numbers, and hence $\delta\Delta H_{red}$-values. These different flow situations are treated in the following sections.

Case I (Fig. 1 a): $\lambda_1 \ll b \gg a$. This condition implies also that the chamber flow Knudsen number $Kn_1 \ll 1$. In all instances the flow in the chamber behaves therefore as a continuum flow.

The nature of the channel flow depends on the channel Knudsen number Kn_2. In the channel there is either a transition from viscous, incompressible flow to viscous, compressible flow or viscous slipping flow, or, if $Kn_2 \gg 1$, to free molecular flow.

The flow in the chamber, however, is purely viscous and the mass flow velocity is uniform and small ($Ma_1 < 1/3$), except for the flow in the high velocity region. The static external pressure exerted on the sample surface is therefore also uniform and approaches the stagnation pressure. Consequently, the effect on the vaporization enthalpy will be small. Its magnitude can be estimated from eqn. (13) for the region $0 < Ma_1 < 1/3$ and is found to be $0 < \delta\Delta H_v(25°C) <$ *ca.* 30 cal/mole.

Case II a (Fig. 1 b): $b=0$, $a>h$, $\lambda_1 < d < h$. The first two conditions imply that the vapor phase in contact with the evaporation surface is no longer uniform in respect to pressure, density, and temperature, because part of the evaporating surface has deeply entered into the high-velocity region.

† The suffix 2 refers to channel flow.

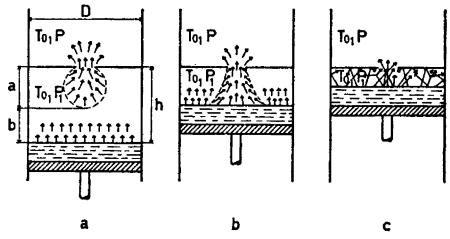

Fig. 1. Open system models for different flow patterns: a) viscous incompressible, b) viscous compressible, and c) molecular flow.

The third condition implies that the vapor in the chamber as well as in the flow channel is still in the continuum region.*

Since that particular portion of the surface area upstream from the flow channel is exposed to a flow region, in which the Mach number approaches unity, the rate of evaporation approaches, according to Crout's theory, its maximum value. As a consequence, there will be a disproportionately larger contribution of evaporated molecules to the total mass flow from that portion of the surface than from the remainder, which is exposed to a flow region with, say, $0<\mathrm{Ma}<1/3$. Hence, the effect of the mass flow upon the static external pressure is primarily restricted to that particular portion of the surface area, whereas the static external pressure on the remaining surface area is affected to approximately the same extent as in case I.

It is clear, that under such circumstances the enthalpy of vaporization is strongly affected. When the flow velocity in the chamber has become sonic ($\mathrm{Ma}_1=\mathrm{Ma}_2=1$) the limiting value for $\delta\Delta H_v$ is, from eqn. (13), equal to *ca.* 230 cal/mole at 25°C. Since, however, the flow velocity cannot become purely sonic throughout the *total* flow region, comprising both the chamber and the channel, the actual $\delta\Delta H_v$-value must be expected to be somewhat reduced.

Case II b (Fig. 1 c): $b=0$, $a>h$, $\lambda_1\geq d\approx h$, $0\leq l/d\lesssim\lambda_1/d$. This case differs from the preceding one in the third condition: the Knudsen number exceeds unity both for the chamber and for the channel. A further restriction is imposed by the fourth condition which implies that the vapor flow through orifices and very short tubes only is being considered. According to Sreekanth's experiments,[22] the flow downstream of an orifice is for Knudsen numbers 0.3—0.5 still very close to a continuum type jet. When $\mathrm{Kn}=2$ almost free molecular flow conditions prevail. Within these limits the transition from isentropic continuum expansion to non-isentropic free molecular expansion has definitely occurred.

The circumstance that $\mathrm{Kn}_0\approx\mathrm{Kn}_1\approx\mathrm{Kn}_2\gtrsim 1$ must have a noticeable effect on the characteristics of flow through orifices and short pipes, differing in several aspects from the behavior of the flows considered in case II a.

For the first, the vapor molecules will now not be able to adapt themselves to equilibrium conditions within the boundaries of the vaporization chamber,

* However, it must be remembered that the mean free path λ_0 of the stagnation vapor will, in the course of the isentropic expansion, increase [13] (for $K\rightarrow 1$ and $\mathrm{Ma}_1=1$, $\lambda_1=2.7\lambda$).

because the time spent in the chamber and channel together will be shorter even than the relaxation time of the translational degrees of freedom.

For the second, it is obviously possible for a number of molecules to leave the chamber immediately after evaporation without encountering any intermolecular collision in the chamber and the channel on their exit. This number may be appreciable [13] even for $Kn \leq 1$.

It is clear, that under these special circumstances the random motion of the molecules in the flow direction over a distance of one to two mean free paths from the evaporating surface is somewhat reduced. Using Crout's terminology, this situation would be equivalent to a diminishing of the longitudinal temperature as compared with the transversal temperature. It follows that one may also define two different velocities of sound, and as a consequence, two different flow Mach numbers to the mass flow away from the surface: a longitudinal and a transversal Mach number. Since the Mach number represents the ratio of mass flow velocity to sound velocity and since the largest contribution to the total mass flow comes from the longitudinal motion of the molecules, it becomes apparent that the overall Mach number of the flow on its passage out of the chamber may considerably exceed unity.

In the extreme case, when $Kn_1 \rightarrow \infty$ and the molecular motion in the beam is primarily longitudinal, the flow Mach number approaches infinity. For an isotropic gas this situation will be realized when the total kinetic energy of the gas has become unidirectional. The flow velocity [6] then has reached its maximum value $(2RT_0/M)^{\frac{1}{2}}$.

Obviously, the value of $\delta \Delta H_v$ exceeds under the above stated conditions the maximum value for isotropic vapor flow and approaches the limiting value RT_0. From formula (13) it can be calculated that this value may probably be reached, within the limits of experimental errors, already at a longitudinal Mach number $Ma \approx 2.5$.

The problems considered here may, however, also be approached in a different way. It has been shown that a decrease in the PV-work of the evaporating molecules will affect the enthalpy of vaporization. This PV-work is the work done by the evaporated molecules in pushing the bulk of the vapor ahead of themselves in a direction normal to the evaporating surface. On a molecular scale this work will be realized by means of intermolecular collisions. If now a number of freshly evaporated molecules pass through a finite volume element without colliding, there can be no talk of a PV-work performance on their behalf. Hence, the overall PV-work will be smaller than RT_0. If the number of non-colliding molecules is much larger than the number of colliding molecules, the PV-work approaches zero, *i.e.* $\delta \Delta H_{red}$ tends to unity.

INSTRUMENTATION

Two of the main purposes with the new, redesigned apparatus were to minimize heat leakages from the surroundings to the calorimeter and to obtain boundaries of well defined geometry within the calorimetric system, in order to define more precisely where the calorimeter proper ends and the surrounding jacket begins. Hence to realize these intentions it was decided

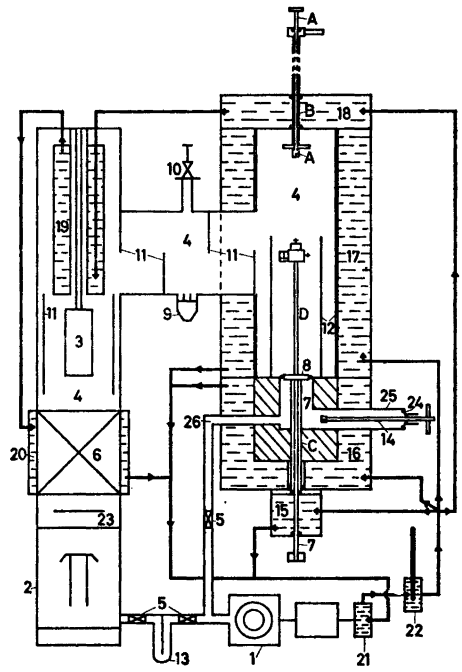

Fig. 2. Simplified cross-sectional view of the assembled apparatus.

to position the calorimeter directly in the high-vacuum line, supported by a long thin-walled evacuated and thermostatted stainless steel tube and surrounded from all sides by thermostatted walls.

Vacuum-system. The high-vacuum system (Fig. 2) was largely constructed by means of commercially available parts (Leybold system), consisting of a rotary oil fore-pump (1), a two-stage oil diffusion pump (2), a liquid nitrogen trap in stainless steel (3) (volume *ca.* 500 ml), the vacuum line of steel pipes with an inner diameter of 100 mm (4), and the necessary valves (5), partly assembled in a one-handle combination block (6), a sluice chamber (7), a sluice valve (8), an ionization gauge (9), a precision dosaging valve for the continuous variation of the residual pressure (10), radiation shields (11) for the cold trap and for the calorimeter (12), and a solid carbon dioxide trap (13) placed between diffusion pump and fore-pump. The vacuum line and the ionization gauge were supplied with facilities for outheating. The whole system was kept under a steady high-vacuum by means of electrical and electronic relays (not shown in Fig. 2) controlling the flow of cooling water to the diffusion pump and the pressure in the line, respectively. The lowest pressure obtained, as indicated by the ionization gauge, was 2×10^{-6} mm Hg.

Calorimetric apparatus. The dimensions and the design of the calorimeter are principally the same as for the calorimeter previously described.[1] The calorimeter support, however, is completely changed. The most important improvements are the following: a) the calorimeter is fitted directly with a temperature sensor (thermistor) fixed in a central position close to the evaporating sample; b) the electrical heater is soldered directly to the silver bottom plate of the evaporation chamber; c) all components in the vicinity of the sample were either constructed of silver or heavily silvered (electrochemically); d) all the interchangeable flow channels employed can be vacuum-tightly fitted into the outlet tube of the calorimeter, thus ensuring reproducible flow measurements; e) thermal contact of the calorimeter and the calorimeter support with the outside is

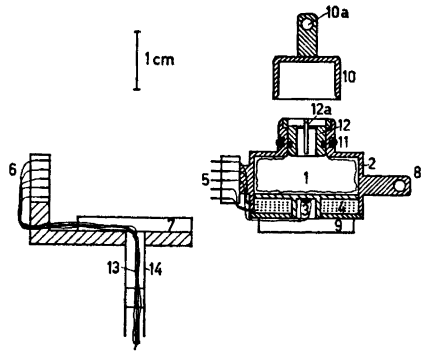

Fig. 3. Cross-section of the vaporization calorimeter and calorimeter holder.

minimized by fixing the support on top of a pipe (*ca.* 40 cm long, 6 mm outer diameter, wall thickness 0.4 mm) of bad heat conducting material (stainless steel); the pipe contains all the electrical leads to the calorimeter.

In Fig. 3 a cross-section of the calorimeter, the calorimeter support and a flow channel are depicted.

The calorimeter consists of a thin-walled cylindrical brass shell (2) with a wall thickness of 0.5 mm. The shell encloses the vaporization chamber (1), whose interior diameter is 16 mm, and the outlet tube of diameter 6.5 mm. In the chamber section is soldered a 2 mm thick bottom plate, the surface of which is roughened by course graining. Both the interior brass walls and the silver bottom plate are silvered. The silver bottom plate contains in its center a small circular cavity in which a thermistor (Stantel M52, bed type, *ca.* 3850 ohms at 25°C) is fixed by means of shellac (3). The electrical heaters (4) (a 50 ohms "main" heater and two 25 ohms "auxiliary" heaters) are soldered onto the bottom using Rose's metal (m.p. *ca.* 110°C). The heaters form a spiral around the thermistor.

In order to make electrical connections to the outlet leads (13) in the supporting pipe (14), the copper leads of the heaters and the thermistor (in all 14 leads) are connected to the male joints (5) of a 3 × 5-pole micropole-plug fixed on the side wall of the calorimeter. The female section (6) is fixed in a holder in the calorimeter support (7).

Opposite to the micro-plug the calorimeter wall is furnished with a simple bayonet-joint (8) by means of which the calorimeter can be fixed to a horizontal operating rod (14, Fig. 2).

The lower end of the brass shell is closed with a 2 mm thick outer bottom brass plate, soldered with Rose's metal. It is furnished with a dove-tail (9) which connects the calorimeter to the calorimeter support. By means of this dove-tail the calorimeter is kept in position when the calorimeter lid (10) is lifted off at the beginning of an experiment.

The lid is made in brass and can be connected to a vertical operating handle (A, Fig. 2) *via* a bayonet joint (10a). The vacuum-tight fitting of the lid was achieved by means of a hard nitrile rubber O-ring seal (11) and by a proper dimensioning of the interior lid diameter, which made it possible to achieve a minimum radial contact area between the polished lid and the seal. The interior surface area of the lid is smeared with vacuum grease, which is subsequently removed with a tissue. Hence a thin grease film is left covering the tightening surface area.

This treatment guarantees the almost frictionless removal of the lid. Experimentally it is found that the temperature change produced by frictional heat does not exceed 3×10^{-4}°C which corresponds to approximately the same figure in calories (the heat capacity of the calorimeter was experimentally found to be *ca.* 0.8 cal·degree^{-1}).

The interchangeable flow channel holders have the shape indicated (12). They are made in brass and furnished with a tiny rubber O-ring seal. The following six channel types are employed:

a) *glass capillaries;* b) *stainless steel pipes;* c) *orifices;* prepared by drilling circular holes in the center of 5 mm diameter stainless steel sheets, either 0.020 or 0.012 mm in thickness; d) *multi-parallel quadratic orifices* (400 mesh); e) *50 μ-diameter blend;* f) in a few cases, where large orifices were needed, the previously described *orifice plates* are used [1] (lip thickness *ca.* 0.1 mm).

All metal channels (except f) are soldered in the holder top plate (12a). In Table 1 the dimensions of the channels employed are given. The diameters are measured by means of a calibrated optical microscope.

Variations in the calorimeter weight. A few organic materials were used for the construction of the calorimeter which caused variations in the calorimeter weight, as a result of desorption and absorption effects. These were dependent upon the time during which the calorimeter was under high-vacuum and under atmospheric pressure, respectively. It could be proved that the time- dependence and the magnitude of these sorption effects were reproducible.

Table 1.

Channel number	diameter (mm)	l/r
K 1	0.13	
K 3 [a]	0.26	45.1
K 4	0.36	$33._5$
K 5	0.42	$28._6$
K 6	0.49	$26._6$
K 7	0.60	$22._4$
K 8	0.66	$21._0$
K 9	1.09	$12._8$
K 10	1.60	$8._6$
K 11	0.79	$17._2$
K 12	0.58	$11._1$
K 14	0.63	$11._1$
K 17	1.18	$11._9$
K 18	1.22	$11._5$
K 19	1.26	$11._1$
K 25	0.89	7.8_9
K 26	0.93	7.5_2
Gl 3 [b]	0.16	79
Bl 50 [c]	~0.05	~ 4
Or 3 [d]	0.55	0.043_6
Or 5	0.32	0.12_3
Or 6	1.46	0.016_5
Or 7	2.20	0.010_9
Or 8	0.10	0.024
Or 9	0.91	0.026_5
Or 10	1.92	0.012_5
Or I [e]	1.5	
Or II	2.6	
Or III	2.4	
Gr I [f]	0.03	

[a] K = stainless steel canule;
[b] Gl = glass capillary;
[c] Bl = electron microscope blend;
[d] Or = orifice;
[e] Or + Roman fig. = old type brass orifice;
[f] Gr = electron microscope grids, 400 mesh.

Hence, it was necessary to perform a series of calorimetric measurements strictly according to some time-schedule. It was found that for repeated sequences of a period of 75 min duration under high-vacuum and 2 min in the atmosphere the calorimeter weight became reproducible from the third measurements onwards, to within *ca.* ± 15 μg. During the latter period the weight was read off after exactly 1 min.

Thermostatting of the calorimeter. At an early stage it was found that it was very difficult to maintain isothermal conditions by employing a liquid nitrogen trap in order to prevent sample vapors from entering the oil diffusion pump as the calorimeter proved to be very sensitive to heat exchanges by radiation (optimal achievable temperature constancy: 5×10^{-4}°C during *max.* 2 h). It was therefore decided to use the trap only on special occasions. Instead of condensing the sample vapor before reaching the diffusion pump, they were directly passed through the pump, and then condensed on a trap charged with solid CO_2. By inspection it was found, after *ca.* 200 experiments, that only a small amount of the vapors had been cracked.

Without the liquid nitrogen trap the calorimeter temperature did not change by more than 3×10^{-4}°C during 24 h. The short-time constancy was about 10^{-5}°C, provided that the cooling water was roughly thermostatted to within *ca.* 0.5°C.

In Fig. 2 the main parts of the thermostat are shown.

In principle, the thermostat is a closed system, comprising six separate thermostatted sections (15—20), through which water at 25°C is pumped *via* a small water turbine (21). The total amount of water in the system is *ca.* 10 l. The circulation rate (at the turbine outlet) is *ca.* 20 l·min^{-1}.

Three sections are coupled in series (18, 19, 20), whereas this combination and the remaining three sections (15, 16, 17) are coupled in parallel. This arrangement was necessary in order to supply the four most important sections (15, 16, 17, 18) simultaneously with water of the same temperature.

All main sections, as well as the extending parts of the vacuum line are heat-insulated by means of quartz wool and styrofoam. The thermostat can be operated in the temperature range 25°—75°C.

At 25°C the temperature variations in the water are about ±0.004°C, as previously stated, on the vacuum-line inside wall, however, the variation is less than *ca.* 0.001°C. This is probably due to the damping effect displayed by the large metal mass of the line (*ca.* 36 kg) and by the relatively large circulation speed.

Temperature controlling system. The temperature of the calorimeter was controlled by means of a thermistor (Stantel M 53, bead type, *ca.* 3850 ohms at 25°C) in a conventional Wheatstone bridge circuit furnished with an amplifier (Tinsley Galvanometer Photocell Amplifier) and a galvanometer follower (Sefram, Paris, Suivier de Spot Photodyne), which registered the temperature variations. The amplification was adjusted to a value corresponding to a sensitivity of 5×10^{-5}°C/mm deflection. The bridge was supplied from a storage battery (2 V, 180 Ah), and the bridge current was adjusted to 100 μA.

Electrical energy measuring system. The vaporization heat was compensated by electrical energy. A known constant current was passed through the main heater for a known period of time. In order to meet small variations in the vaporization rate, requiring correspondingly small heat input changes, stepwise changeable electrical energy was simultaneously supplied to the auxiliary heater from an energy dividing unit (described in detail elsewhere [24]).

The accuracy of the energy dividing unit is found to be better than 0.05 %, and the overall error in the measurement of the total amount of electrical energy is estimated to be 0.1 % or slightly better.

EXPERIMENTAL PROCEDURE

The calorimeter was kept in the high-vacuum chamber (4, Fig. 3) over night, with the lid withdrawn and suspended. Next morning the open calorimeter was moved to the sluice chamber, in which the pressure was raised to 1 atm. Simultaneously a stopwatch was started. The calorimeter was then removed from the system and charged with *ca.* 0.10 to 0.15 ml substance by means of a syringe. (If the substance was solid, a small amount, *ca.* 0.3 g, was melted and then poured into the calorimeter.) An appro-

priate flow channel was inserted (12, Fig. 3) and the calorimeter was attached to the calorimeter support (7, Fig. 3) in the sluice chamber. Both the sluice chamber and the calorimeter were evacuated after exactly 2 min had passed. At the same time the stop-watch was reset. The calorimeter was then moved to its experimental position in the high-vacuum chamber and closed. The handle (A, Fig. 2) was left connected with the lid. Finally, the calorimeter was electrically heated to slightly above the surrounding temperature and allowed to equilibrate.

During 60 min, absorbed gases were desorbed and the calorimeter was opened. During the following 10 min substance was vaporized and the steady state main current adjusted by means of a rheostat. The resulting rheostat position was maintained during the series of calorimetric measurements. Then the calorimeter was closed again and moved to the sluice chamber. When the pressure in the latter was raised to 1 atm, a stop-watch was started and the calorimeter immediately transferred to the micro-balance. After exactly 60 sec the weight was read off and the calorimeter again moved to the sluice chamber and placed on the calorimeter support. After exactly 120 sec had passed the pressure was reduced to fore-pump pressure and the calorimeter placed again in its experimental position in the high-vacuum chamber. Since, owing to the expansion of the air in the sluice chamber, the calorimeter was cooled, it was electrically heated to a temperature slightly above equilibrium temperature and then allowed to equilibrate.

After 60 min the calorimeter was ready for the first measurement. The auxiliary energy-time recorder was started, and when the pen passed a previously asserted zero point, both the initially adjusted main heating current and the largest auxiliary current were switched on and the stop-watch was started. After a few seconds the calorimeter temperature was raised by *ca.* 0.005°C. Then the lid was pulled off. Under the action of the unbalanced pressure forces the vapor suddenly started to flow through the flow channel at a considerably higher initial velocity than the steady state velocity. Subsequently, an expansion wave swept through the calorimeter vapor space thus causing a rapid vaporization as a result of which the calorimeter cooled. Just before the temperature had dropped *ca.* 0.005°C below the equilibrium temperature, the lid was loosely placed on the calorimeter and thus the vapor flow was choked. The temperature rose again to slightly above the equilibrium value (*ca.* +0.001°C). Then the same procedure with opening and closing the calorimeter was repeated. Usually after 30 to 90 sec steady state conditions were established and from then on the temperature was kept constant to within $\pm 5 \times 10^{-5}$ °C by changing the auxiliary current, if necessary. During the starting vaporization period an attempt was made to perform the vaporization in such a way that the temperature-time curve, as recorded by the galvanometer follower, displayed almost equal areas below and above the zero-line. Using this procedure the gain and loss of heat by exchange with the surroundings nearly counter-balanced each other.

At the end of the measuring period, *i.e.* after 10—30 min, the calorimeter was closed, removed and weighed in the same manner as described previously. A subsequent experiment could be started immediately, according to the time-schedule indicated. With one charge a sequence of 3 to 6 (sometimes more) experiments could be performed. After a series of measurements were finished the calorimeter was opened in the high-vacuum chamber and cleaned by evaporating completely all remaining substance.

MATERIALS

Alkanes. The alkanes previously used [1] were used again, including also *cyclohexane*, *3-methyl-pentane*, and *hendecane* (purity by GLC > 99.9 % > 99.9 % and 99.9 %, respectively).

Xylenols. Purum grade (Fluka) samples of *2,4-xylenol* (*l*), *2,6-xylenol* (*s*), *and 3,4-xylenol* (*s*) were purified by fractional distillation and zone-melting, respectively. Purity of 2,4-xylenol by GLC: 99.8 %; melting points of 2,6- and 3,4-xylenol: 45.5—45.7°C and 65.1—65.2°C, respectively; lit.: 45.62°C and 65.11°C, respectively.[25]

Water. Freshly glass distilled water was used.

Table 2.

Substance	Series No.	ΔH_v (obs) kcal·mole^{-1}	Stand.dev. S[$\Delta H_{v(obs)}$] kcal·mole^{-1}	Flow [a] channel No.	m μ-mole sec^{-1}	Vaporization time min	$\delta\Delta H_v$ kcal·mole^{-1}
Cyclohexane $\Delta H_v = 7.90$ kcal·mole^{-1} $P_0 = 97.5$ mm Hg	1(4)	7.88	0.01_3	K 1 [b]	0.74214	12	0.02
3-Methyl-pentane $\Delta H_v = 7.24$ kcal·mole^{-1} $P_0 = 190.0$ mm Hg	2(2)	7.24	0.03_5	K 1 [c]	0.76003	12	0.00
Water [d]	3(6)	10.52	0.01_0	Bl 50	0.47396	23	0.00
$\Delta H_v^g = 10.52$ kcal·mole^{-1}	4(7)	10.29	0.00_4	Bl 50	0.46355	25	0.23
$P_0^h = 23.76$ mm Hg	5(6)	10.50	0.01_8	G 1	0.60135	25	0.02
Octane	6(3)	9.91	0.02_0	Bl 50	0.11260	14	0.01
$\Delta H_v = 9.92$ kcal·mole^{-1}	7(6)	9.90	0.01_0	K 4	0.16085	12	0.02
$P_0 = 14.0$ mm Hg							
Decane	8(3)	12.08	0.01_9	K 3	0.034656	35	0.20
$\Delta H_v = 12.28$ kcal·mole^{-1}	9(11)	12.11	0.01_7	K 4	0.10762	15	0.17
$P_0 = 1.30$ mm Hg	10(5)	12.19	0.00_7	K 5	0.16708	12	0.09
	11(6)	12.25	0.00_5	K 6	0.28306	10	0.03
	12(3)	12.05	0.03_0	Or 8	0.17362	11	0.23
Hendecane	13(4)	13.25	0.03_9	K 6	0.04670	20	0.21
$\Delta H_v = 13.46$ kcal·mole^{-1}	14(5)	13.25	0.02_6	K 7	0.088060	15	0.21
$P_0^i = 0.39$ mm Hg	15(4)	13.25	0.01_1	K 8	0.10628	15	0.21
	16(5)	13.36	0.02_1	K 12	0.13228	11	0.10
	17(5)	13.45	0.01_0	K 11	0.21112	10	0.01
	18(4)	13.38	0.02_2	K 14	0.16169	13	0.08
	19(5)	13.32	0.00_8	K 14	0.16160	10	0.14
	20(3)	13.26	0.02_9	K 14	0.16126	10	0.20
Dodecane	21(6)	14.44	0.02_0	K 25	0.008844	12	0.21
$\Delta H_v = 14.65$ kcal·mole^{-1}	22(3)	14.44	0.01_7	K 26	0.010167	15	0.21
$P_0^i = 0.12$ mm Hg	23(3)	14.44	0.04_5	Or 5	0.043237	25	0.21
	24(4)	14.54	0.02_1	Or 3	0.10989	15	0.09
	25(3)	14.44	0.01_5	Or 3	0.10901	15	0.21
	26(5)	14.45	0.02_1	K 17	0.13639	12	0.20
	27(5)	14.44	0.00_9	K 18	0.13966	11	0.21
	28(4)	14.41	0.01_6	K 19	0.16188	10	0.24

Table 2. Continued.

Substance	Series No.	ΔH_v (obs) kcal·mole^{-1}	Stand.dev. $S[\Delta H_{v(obs)}]$ kcal·mole^{-1}	Flow [a] channel No.	m μmole sec^{-1}	Vaporization time min	$\delta\Delta H_v$ kcal·mole^{-1}
Tetradecane	29(5)	16.80	0.03_2	Or 6	0.062056	15	0.21
$\Delta H_v = 17.01$ kcal·mole^{-1}	30(6)	16.80	0.02_3	Or III	0.10282	15	0.21
$P_0^{i} = 0.01$ mm Hg	31(3)	16.83	0.00_7	Or II	0.22192	10	0.18
	32(6)	16.62	0.03_6	Or 9	0.024198	37	0.39
	33(6)	16.64	0.03_5	Gr I	0.057081	15	0.37
Hexadecane	34(3)	19.04	0.01_1	open [e]	0.066554	15	0.34
$\Delta H_v = 19.36$ kcal·mole^{-1}	35(8)	19.01 [f]	0.05_1	open [e]	0.095441	10	0.33 [f]
$P_0^{i} = 0.001$ mm Hg	36(5)	18.80 [d]	0.00_2	open [e]	0.022544	35	0.58
	37(2)	18.7_7 [d]	0.04	Or I	0.005563	120	0.6
2,6-Xylenol, solid	38(4)	17.85	0.04_5	K 11	0.05153	20	0.23
$\Delta H_v = 18.08$ kcal·mole^{-1}	39(6)	17.96	0.01_2	K 9	0.12953	15	0.14
$P_0 = 0.18$ mm Hg	40(6)	18.00	0.03_2	K 18	0.18046	11	0.08
2,4-Xylenol, liquid	41(4)	15.52	0.04_0	K 9	0.05732	25	0.24
$\Delta H_v = 15.76$ kcal·mole^{-1}	42(8)	15.53	0.01_1	K 10	0.19690	12	0.25
$P_0 = 0.10$ mm Hg							
3,4-Xylenol, solid	43(4)	20.31	0.03_5	Gr I	0.062269	23	0.20
$\Delta H_v = 20.51$ kcal·mole^{-1}	44(5)	20.30	0.01_7	Or 10	0.13102	11	0.21
$P_0 = 0.01$ mm Hg	45(3)	20.30	0.03_1	Or II	0.21080	20	0.21

[a] See Table 1.
[b] The conductance of the channel was reduced by inserting a 0.06 mm diam. Ni-wire.
[c] As *b*), but wire diameter 0.1 mm.
[d] Liquid nitrogen trap was used.
[e] The outlet tube of the calorimeter was used as flow channel.
[f] Thermostat temperature 27.3°C. By Watson's formula [26] ΔH_v was calculated to be 19.33 kcal·mole^{-1}.
[g] Ref. 28; all remaining data on vaporization enthalpies (25°C) from Ref. 25.
[h] Ref. 27; remaining vapor pressure data (25°C) from Ref. 25.
[i] Extrapolated values from a plot of log P_0 *versus* chain length.

RESULTS

The results from 45 series of measurements are compiled in Table 2. Column 1 gives the name of the substance, the vapor pressure, and the literature vaporization enthalpy, column 2 the series number and in brackets the number of measurements, column 3 the computed mean value of the vaporization enthalpy, column 4 its standard deviation (for 5 or more measurements) or its mean average deviation (for less than 5 measurements); column 5 indicates the flow channel used (see also Table 1), column 6 the average mass flow, and column 7 the duration of a measurement.

A seventh column is added showing the reduced difference between the literature datum and the experimental value of the vaporization enthalpy.

DISCUSSION

Since neither the static external pressure nor the flow Mach number in the chamber could be measured directly, it was impossible to check the correctness of either eqn. (8) or eqns. (12) and (13) immediately. It should, however, be possible to check whether the experimental results reflected the

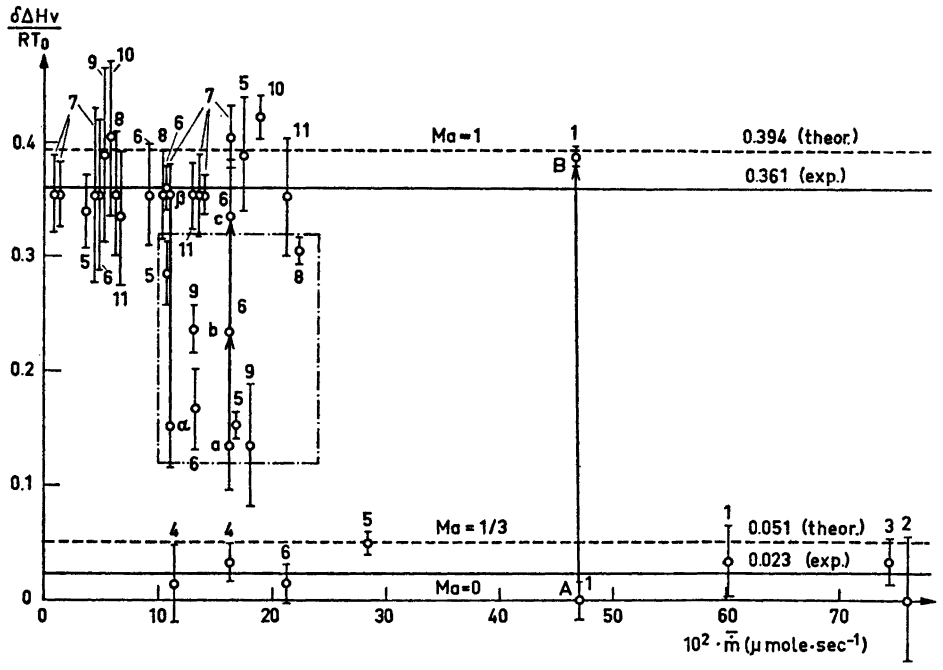

Fig. 4. Diagram of reduced ΔH_v-difference *versus* average mass flow (*Mach number range* $0 \leq Ma \leq 0.5$). 1, water; 2, 3-methylpentane; 3, cyclohexane; 4, octane; 5, decane; 6, hendecane; 7, dodecane; 8, tetradecane; 9, 2,6-xylenol; 10, 2,4-xylenol; 13, 3,4-xylenol.

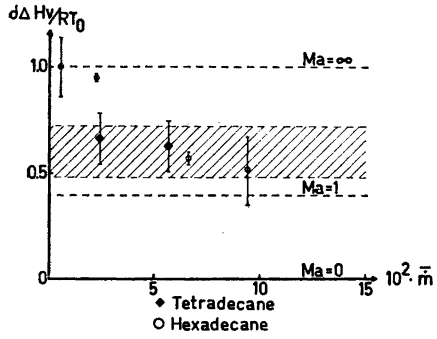

Fig. 5. Diagram of reduced ΔH_v-difference *versus* average mass flow (*Mach number range* $0 \leq Ma \leq 1.2$).

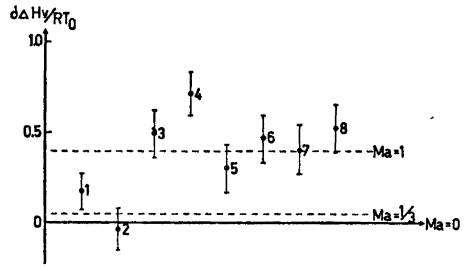

Fig. 6. McCurdy's and Laidler's data plotted as reduced ΔH_v-differences *versus* substance, see Table 3 (*Mach number range* $0 \leq Ma \leq 1$).

limiting values calculated for the different model cases. In Figs. 4 and 5 diagrams of the reduced differences $\delta\Delta H_{red}$ between the literature data and experimental data are plotted *versus* the average mass flow $\dot{m}$ (μmole·sec^{-1}) with the reduced standard deviation attached to the points (vertical lines).

Fig. 4 shows the range $0 \leq \delta\Delta H_{red} \leq 0.5$, which according to eqn. (13) corresponds to the Mach number range $0 \leq Ma \leq ca.$ 1.2. The limiting lines for sonic flow ($Ma=1$, $\delta\Delta H_{red}=0.394$) and for incompressible flow ($0<Ma<1/30, <\delta\Delta H_{red}<0.051$) were drawn.

It is obvious that the majority of the reduced differences (23 points) is located in close proximity to the unity Mach number line. Their mean value is calculated to be 0.361 ± 0.018 (av.dev.). It seems that the difference of *ca.* 8 % between the theoretical value (for $K \rightarrow 1$) and the experimental value is practically insignificant; a slight difference was, however, expected, as mentioned above. It is to be noted that the difference is in the predicted direction.

Eight points fall in the region for incompressible flow and are located in the Mach number range $0<Ma<1/3$. Their mean value is equal to $\delta\Delta H_{red}=0.023 \pm 0.016$ (*av.dev.*). These points were obtained from measurements on substances in the vapor pressure range $200>P_0>0.4$ mm Hg, corresponding to the range of mean free paths $6 \times 10^{-6} < \lambda_0 < 1.6 \times 10^{-3}$ cm.

A few points are located in the region between sonic flow and incompressible flow (within rectangular). The appearance of points in that region was expected in those cases, in which the high velocity region of the flow had approached the evaporating surface sufficiently close in order to touch it or to make the surface to ingress the high velocity region. By diminishing the channel entrance-sample surface separation it should then be possible to move a part of the surface entirely into the high velocity region with a resulting increase in the $\delta\Delta H_v$-value and a displacement of the $\delta\Delta H_{red}$-value towards the sonic line in Fig. 4. A few such experiments were performed on water (series 3 and

4), hendecane (series 18, 19, and 20) and dodecane (series 24 and 25). It becomes obvious from the diagram (Fig. 4, arrows) that a displacement really occurred in the correct direction: for water from A (*incompressible flow*) to B (*sonic flow*), for hendecane, in two steps, from a (*compressible flow*) to b (*compressible flow, not yet sonic*) and finally to c (*sonic flow*) and for dodecane from α (*compressible flow*) to β (*sonic flow*). It can be seen that the mass flows were practically unchanged for hendecane and dodecane, and slightly decreased for water.

In Fig. 5 those points are plotted which fall into the range of $\delta\Delta H_{red}$-values corresponding to Mach numbers exceeding unity, *i.e.* $0.394 < \delta\Delta H_{red} < 1.000$, and $1 < Ma < \infty$. These points represent series of measurements on hexadecane (series 34 to 37) and two from a total of five series on tetradecane (series 32 and 33). The vapor pressures of these two substances at room temperature is in the range 10^{-2} to 10^{-3} mm Hg.

For hexadecane the chamber flow Knudsen numbers were *ca.* 0.7 for series 34 and *ca.* unity for the remaining series, whereas the channel flow Knudsen numbers increased from *ca.* 0.7 for series 34 to unity for series 35 and 36 and to *ca.* 6 for series 37. For series 36 and 37 the number of molecules reflected back into the evaporation chamber was reduced by condensing the discharged vapor on the liquid nitrogen trap, but for series 34 and 35 the trap was not used. The effect of the reduction in back reflection is significant as shown from a comparison between the data obtained for series 35 and 36 for which the same flow channel was used: the increase in $\delta\Delta H_{red}$ amounts to 0.375.

When tetradecane was discharged through orifices at Knudsen numbers $0.5 < Kn < 0.8$ (series 29, 30, and 31) the chamber flow velocity was evidently sonic (Fig. 6) and the resulting $\delta\Delta H_{red}$-values were located close to the theoretically calculated value. When the channel Knudsen number, however, was increased (series 32: $Kn_2 = 1.3$, and series 33: $Kn_3 = 4$) a significant increase in the $\delta\Delta H$red-value was obtained.

Thus it seems that the simple theory proposed, together with Crout's theory is able to describe quantitatively, within the experimental uncertainties, the influence which the flow velocity upstream from a discharge flow channel may exert on an evaporating surface and hence on the enthalpy of vaporization. It will therefore also be possible to apply the calorimeter and the method developed with much more confidence than was possible previously to the determination of vaporization enthalpies of foreign substances, both liquids and solids, at room temperature or at an elevated temperature. Furthermore, this theory provides an interpretation of the systematic errors previously observed.[1]

It is obvious, that it is not sufficient to measure the enthalpy of vaporization by only employing a certain flow channel, since from a single series of measurements it cannot be decided what correction has to be applied. It is necessary to perform at least two series of measurements. For one of the series the channel should be placed at a distance, which is large compared with the mean free path, from the sample surface. For the other series the channel, preferably one with a smaller diameter, should be placed in the vicinity of the sample surface.

If the vapor pressure of the investigated substance falls in the high pressure range, *i.e.* $200 > P_0 > ca.$ 10 mm Hg, incompressible chamber flow

may be expected for both series * (*i.e.* $1/3>\mathrm{Ma}>0$). The reduced difference between the obtained data should then not surmount the value 0.051, corresponding to $\mathrm{Ma}=1/3$. The reduced correction to be applied is in this case 0.023 ± 0.016.

If the vapor pressure falls in the medium pressure range, *i.e. ca.* $10>P_0>$ *ca.* 0.1 mm Hg, incompressible chamber flow may be expected for the first series, and sonic chamber flow for the second. The reduced difference between the obtained data should then amount to *ca.* $0.361-0.023=0.338\pm0.034$ (*max. av. dev.*). The reduced corrections to be applied are 0.023 ± 0.016 and 0.338 ± 0.018 for the first and second series, respectively.

If the vapor pressure is in the range *ca.* $0.1>P_0>ca.$ 0.01 mm Hg sonic chamber flow may be expected for both series, *i.e.* $\mathrm{Ma}\rightarrow1$.** The reduced difference between the obtained data should be within the limits of the experimentally found maximum absolute deviations from the reduced mean value for sonic flow, *i.e.* 0.084 (difference between $\delta\Delta H_{\mathrm{red}}$ of series 20 and 42). The reduced correction to be applied becomes then 0.338 ± 0.018.

If, however, the vapor pressure is close to 0.001 mm Hg, it becomes more difficult to evaluate the precise magnitude of the correction to be applied. It seems that one procedure would be to perform one series of measurements by using the calorimeter outlet tube as flow channel and to perform another series using an orifice or, perhaps, a multi-parallel orifice (grids). In this case the experimental data should not differ largely from each other and it seems that a correction corresponding to a reduced difference of magnitude 0.60 ± 0.15 could be safely applied (shaded area in Fig. 5).

Another possibility would be to use the trap during the experiment, because in this case the correction should amount to *ca.* RT_0.

From the results obtained it is obvious that this calorimetric method may be used equally well for liquid and solid substances.***

It is estimated that the overall uncertainty at 25°C in the vapor pressure range 200 to 10^{-2} mm Hg amounts to max. *ca.* ±40 cal/mole, the main contributions coming from the weight uncertainty (*ca.* ±15 cal/mole for 10 mg vaporized) and from the uncertainty of the correction term (*ca.* ±15 cal/mole).

In the vapor pressure range 10^{-2} to 10^{-3} mm Hg the overall uncertainty increases to *ca.* ±80 cal/mole. Now the main contribution arises from the uncertainty of the correction term (*ca.* ±60 cal/mole).

It is clear that the uncertainty of the weight decreases with increasing amount vaporized.

In conclusion, it is of interest to discuss briefly, in view of the present results, a few of Mc Curdy's and Laidler's data [29] for the vaporization enthalpies

* Only under particular conditions is it possible to move the chamber flow Mach number from the region $0>\mathrm{Ma}<1/3$ to $\mathrm{Ma}=1$, as was done for water (calorimeter filled to the outlet tube and flow channel entrance almost touching the sample surface).

** As a consequence of the restricted size of the evaporation chamber it was impossible in this pressure range to reach the Mach number region $1/3>\mathrm{Ma}>0$.

*** When solids were vaporized an interesting observation was made. After a series was finished and the calorimeter opened it was found that from the crystal mass substance had been removed only immediately underneath the flow channel entrance, where a small crater was formed. This observation supports the assumption that a larger contribution to the total mass flow comes from this particular surface region rather than from the remainder.

of a number of alcohols. These authors used for their measurements a differential calorimeter of the Calvet type. The samples were under vacuum (0.5 mm Hg) vaporized at 25°C from one end of a U-tube and condensed at the other end by means of a coolant (liquid air, dry ice-acetone or ice water). A comparison of their results with reliable data recently obtained in this laboratory [30] shows poor agreement except for the two substances exerting the highest vapor pressures, methanol and ethanol (see Table 3).

Table 3.

	Compound	Mc Curdy/Laidler [a] ΔH_v, kcal·mole^{-1}	Wadsö ΔH_v, kcal·mole^{-1}	$\delta\Delta H_v$ kcal·mole^{-1}
1 [c]	Methanol	9.01	8.91 ± 0.02	−0.10 ± 0.06 [b]
2	Ethanol	10.09	10.11 ± 0.02	0.02 ± 0.07
3	Propanol	10.52	10.81 ± 0.03	0.29 ± 0.08
4	2-Methyl-2-propanol	10.72	11.14 ± 0.02	0.42 ± 0.07
5	2-Propanol	11.13	11.31 ± 0.02	0.18 ± 0.08
6	2-Butanol	11.59	11.87 ± 0.02	0.28 ± 0.08
7	2-Methyl-1-propanol	11.91	12.15 ± 0.02	0.24 ± 0.08
8	1-Butanol	12.19	12.50 ± 0.02	0.31 ± 0.08

[a] The overall uncertainty was estimated to 0.5 %.
[b] Sum of the uncertainties.
[c] Refers to Fig. 6.

In Fig. 6 the reduced differences are plotted in a diagram of $\delta\Delta H_{red}$ *versus* the substances, arranged according to increasing ΔH_v (25°). To each point is attached the maximum uncertainty being the sum of the experimental uncertainties claimed by Mc Curdy-Laidler.

It is seen that some of the points group themselves fairly close to the unity Mach number line, except for 2-methyl-2-propanol, which is rather far off. The two points representing methanol and ethanol are fairly closely located to the zero Mach number line and to the line for Ma=1/3, respectively. Since the authors claim negligible heat conductance along the U-tube and negligible entrainment, it will seem that the main reason for the discrepancies must be sought in the reduction of the pressure-volume work due to an increased flow velocity.

Acknowledgements. I wish to express my thanks to professor Stig Sunner for help and encouragement throughout this work. I am indebted to professor Tyllered and civil engineer Leif Hallgren from the Institution for Mechanical Heat and Fluid Flow Theory at Lund Institute of Technology for checking the gas dynamic part of this study. For technical assistance in the construction of the calorimeter the help of Börje Pettersson, Jan-Eric Falk and Jan-Eric Lindahl is gratefully acknowledged.

REFERENCES

1. Morawetz, E. and Sunner, S. *Acta Chem. Scand.* **17** (1963) 473.
2. Rossini, F. D. *Chemical Thermodynamics*, Wiley, New York 1950.
3. Liepmann, H. W. *J. Fluid Mech.* **10** (1961) 65.
4. Probstein, F. *Heat Transfer in Rarefied Gas Flow*, From Clark, J. A. *Theory and Fundamental Research in Heat Transfer*, Pergamon 1963.
5. Liepmann, H. W. and Puckett, A. E. *Introduction to Aerodynamics of a Compressible Fluid*, Wiley, London 1947.
6. Oswatitsch, K. and Kuerti, G. *Gasdynamics*, Academic, New York 1956.
7. Pai, S. *Introduction to the Theory of Compressible Flow*, van Nostrand, Princeton, N.J. 1959.
8. Weissberger, A. *Technique of Organic Chemistry*, Vol. IV, Distillation, Interscience, New York 1965.
9. Hirschwald, W. and Stranski, I. N. *Condensation and Evaporation of Solids, Proc. Intern. Symp. Condens. Evapor. Solids*, Dayton, Ohio 1962.
10. Crout, P. D. *J. Math. Phys.* **15** (1936) 1; Giddings, H. A. and Crout, P. D. *Ibid* **15** (1936) 124.
11. Schrage, R. W. *Interphase Mass Transfer*, Columbia Univ. Press, New York 1953.
12. Sherwood, Th. K. and Cooke, N. E. *A.I.Ch.E.J.* **3** (1957) 37.
13. Patterson, G. N. *Molecular Flow of Gases*, Wiley, New York 1956.
14. Stanton, T. E. *Proc. Roy. Soc.* **A 111** (1926) 306.
15. Sreekanth, A. K. *Phys. Fluids* **8** (1965) 1951.
16. Frössel, U. *Forsch. Gebiete Ingenieurw.* **7** (1936) 75.
17. Jobson, D. A. *Proc. Inst. Mech. Engrs. London* **169** (1955) 767.
18. Bragg, S. L. *J. Mech. Eng. Sci.* **2** (1960) 35.
19. Gurevich, M. I. *Theory of Jets in Ideal Fluids*, Academic, New York, London 1965.
20. Willis, D. R. *AFOSR 64-0858*, Princeton Univ., Report 683, 1964.
21. Schlichting, H. *Boundary Layer Theory*, McGraw, New York 1955.
22. Sreekanth, A. K. *Techn. Rep. No. 86, 1963, D1-82-0322*, Boeing Scient. Res. Lab., Seattle, Washington.
23. Jeans, J. *Kinetic Theory of Gases*, Cambridge Univ. Press 1946.
24. Morawetz, E. and Nakase, Y. *Unpublished.*
25. *Selected Values of Properties of Chemical Compounds* and *Selected Values of Properties of Hydrocarbons and Related Compounds*, API Res. Proj. 44, Carnegie Inst. Technol. Pittsburgh, Pennsylvania.
26. Watson, K. M. *Ind. Eng. Chem.* **32** (1940) 841; **34** (1942) 1072.
27. Dushman, S. *Scientific Foundations of Vacuum Technique*, Wiley, New York 1961.
28. Rossini, F. D., Wagman, D. D., Evans, W. H., Levine, S. and Jaffe, J. *Selected Values of Chemical Thermodynamic Properties, Circular NBS 500*, U.S. Government Printing Office, Washington D.C. 1952.
29. Mc Curdy, K. G. and Laidler, K. J. *Can. J. Chem.* **41** (1963) 1867.
30. Wadsö, I. *Acta Chem. Scand.* **20** (1966) 544.

Received December 19, 1967.